Added value of myocardial blood flow using ^{18}F-flurpiridaz PET to diagnose coronary artery disease: The flurpiridaz 301 trial

Jonathan B. Moody, PhD,[a] Alexis Poitrasson-Rivière, PhD,[a] Tomoe Hagio, PhD,[a] Christopher Buckley, PhD,[b] Richard L. Weinberg, MD, PhD,[c] James R. Corbett, MD,[c,d] Venkatesh L. Murthy, MD, PhD,[c] and Edward P. Ficaro, PhD[a,c]

[a] INVIA Medical Imaging Solutions, Ann Arbor, MI
[b] GE Pharmaceutical Diagnostics R&D, Amersham, UK
[c] Division of Cardiovascular Medicine, Department of Internal Medicine, University of Michigan, Ann Arbor, MI
[d] Division of Nuclear Medicine, Department of Radiology, University of Michigan, Ann Arbor, MI

Received Aug 30, 2019; accepted Dec 9, 2019
doi:10.1007/s12350-020-02034-2

Background. **^{18}F-Flurpiridaz is a promising investigational radiotracer for PET myocardial perfusion imaging with favorable properties for quantification of myocardial blood flow (MBF). We sought to validate the incremental diagnostic value of absolute MBF quantification in a large multicenter trial against quantitative coronary angiography.**

Methods. **We retrospectively analyzed a subset of patients (N = 231) from the first phase 3 flurpiridaz trial (NCT01347710). Dynamic PET data at rest and pharmacologic stress were fit to a previously validated 2-tissue-compartment model. Absolute MBF and myocardial flow reserve (MFR) were compared with coronary artery disease severity quantified by invasive coronary angiography on a per-patient and per-vessel basis.**

Results. **Stress MBF per-vessel accurately identified obstructive disease (c-index 0.79) and progressively declined with increasing stenosis severity (2.35 ± 0.71 in patients without CAD; 1.92 ± 0.49 in non-obstructed territories of CAD patients; and 1.54 ± 0.50 in diseased territories, $P < 0.05$). MFR similarly declined with increasing stenosis severity (3.03 ± 0.94; 2.69 ± 0.95; and 2.33 ± 0.86, respectively, $P < 0.05$). In multivariable logistic regression modeling, stress MBF and MFR provided incremental diagnostic value beyond patient characteristics and relative perfusion analysis.**

Conclusions. **Clinical myocardial blood flow measurement with ^{18}F-flurpiridaz cardiac PET shows promise for routine application. (J Nucl Cardiol 2021;28:2313–29.)**

Key Words: ^{18}F-flurpiridaz • Coronary artery disease • Cardiac PET • Kinetic modeling • Absolute flow • Flow reserve

The authors of this article have provided a PowerPoint file, available for download at SpringerLink, which summarizes the contents of the paper and is free for re-use at meetings and presentations. Search for the article DOI on SpringerLink.com.

The authors have also provided an audio summary of the article, which is available to download as ESM, or to listen to via the JNC/ASNC Podcast.

All editorial decisions for this article, including selection of reviewers and the final decision, were made by guest editor Henry Gewirtz, MD, PhD.

Venkatesh L. Murthy and Edward P. Ficaro have equal contribution as co-senior authors.

Electronic supplementary material The online version of this article (https://doi.org/10.1007/s12350-020-02034-2) contains supplementary material, which is available to authorized users.

Reprint requests: Jonathan B. Moody, PhD, INVIA Medical Imaging Solutions, 3025 Boardwalk Street, Suite 200, Ann Arbor, MI 48108; *jmoody@inviasolutions.com*

J Nucl Cardiol 2021;28:2313–29.
1071-3581/$34.00

Abbreviations

PET	Positron emission tomography
MBF	Myocardial blood flow
MFR	Myocardial flow reserve
CAD	Coronary artery disease
ICA	Invasive coronary angiography
SPECT	Single photon emission computed tomography

See related editorial, pp. 2330–2334

INTRODUCTION

^{18}F-Flurpiridaz is a promising investigational radiotracer for myocardial perfusion PET with favorable properties for quantification of myocardial blood flow (MBF) and reserve (MFR).[1–3] One phase 3 clinical trial has been completed (''301 trial''[4]) which established the diagnostic performance of flurpiridaz PET myocardial perfusion imaging,[5] and a second phase 3 trial is currently underway (''303 trial''[6]). Several animal studies have demonstrated excellent tracer extraction and have developed kinetic models using microsphere-derived flow measurements as the gold standard.[7–9] In addition, the feasibility of flow measurements in humans has been shown in a small, single-center study.[10] Prior studies, primarily single-center, with ^{13}N-ammonia,[11–13] ^{15}O-water,[14,15] and ^{82}Rb[16,17] have shown that quantification of stress MBF and MFR improves diagnostic

Figure 1. Case examples. **A** female patient, age 60, BMI ▶ 51 kg·m^2, with chest pain, multiple risk factors (hypertension, hypercholesterolemia, diabetes, smoking), and history of PCI to the LAD. Quantitative coronary angiography showed a 92% lesion in the proximal LAD, 88% lesion in the proximal LCX, and a 40% lesion in the mid RCA. ^{18}F-flurpiridaz PET showed a large reversible defect in the LAD territory with coronary steal apparent in absolute flow but not relative retention polar maps, as well as globally and regionally reduced stress flow and flow reserve. Summed static images (2-15 minutes) are shown in the upper left, and kinetic fits to global LV time-activity curves (yellow points and lines) are shown in the bottom right. **B** male patient, age 50, BMI 16 kg·m^2, asymptomatic, multiple risk factors (hypertension, diabetes, smoking), and abnormal baseline EKG. Quantitative coronary angiography showed a 28% lesion in the proximal LAD, 100% lesion in the mid LCX, and an 82% lesion in the mid RCA. ^{18}F-flurpiridaz PET showed a partially reversible defect in the distal LCX and RCA territories, as well as regionally reduced flow and flow reserve in the LCX and RCA territories.

Table 1. Patient characteristics

N (%)	No obstructive CAD (N = 131)	CAD[a] (N = 100)	*P* value
Age, mean ± SD years	61 ± 9	64 ± 10	0.015
BMI, mean ± SD kg·m^2	31.9 ± 5.9	31.0 ± 5.9	0.241
Patient sex			
Male	78 (60)	83 (83)	< 0.001
Female	53 (40)	17 (17)	< 0.001
Obese	76 (58)	55 (55)	0.647
LVEF, mean ± SD %	58 ± 12	56 ± 11	0.092
Family history of CAD	74 (56)	57 (57)	0.938
Hypertension	111 (85)	89 (89)	0.346
Hypercholesterolemia	108 (82)	92 (92)	0.035
Diabetes	41 (31)	45 (45)	0.033
Smoking	72 (55)	65 (65)	0.124
History of MI	12 (9)	24 (24)	0.002
History of PCI	31 (24)	45 (45)	< 0.001
Pre-test likelihood of CAD			
Low	12 (9)	14 (14)	0.249
Intermediate	71 (54)	37 (37)	0.009
High	48 (37)	49 (49)	0.059
Coronary Angiography			
1-vessel CAD	-	65 (65)	-
2-vessel CAD	-	27 (27)	-
3-vessel CAD	-	8 (8)	-

[a]Obstructive CAD was defined by ≥ 50% diameter stenosis

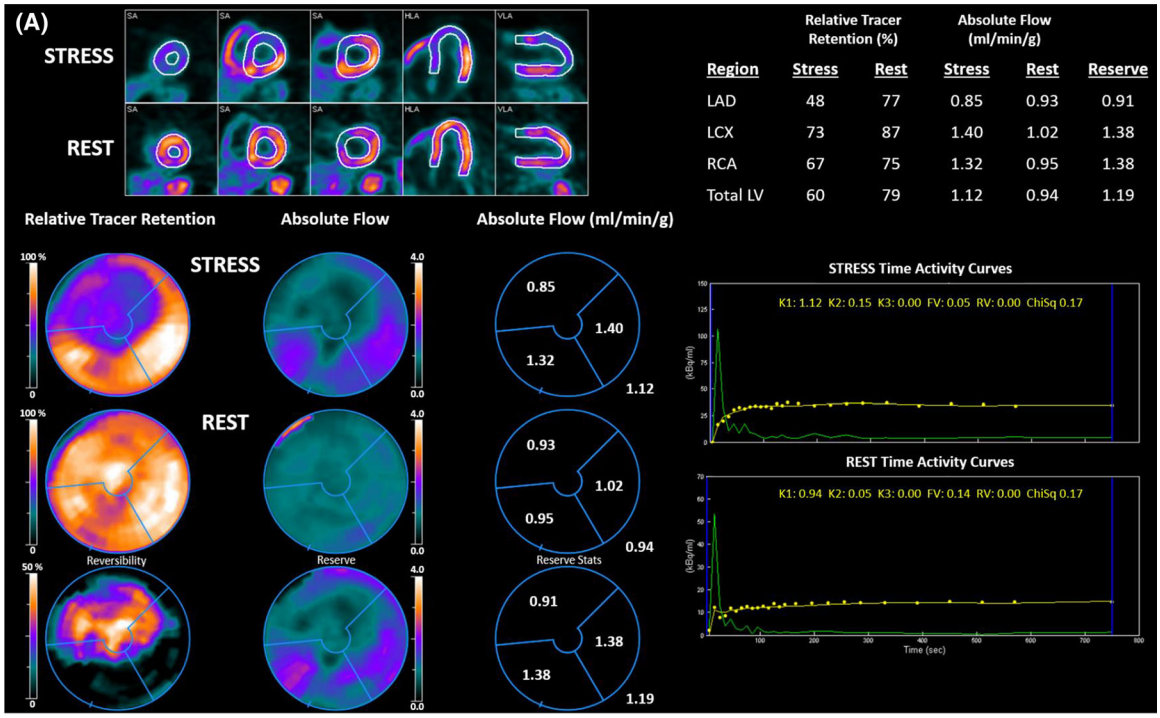

Region	Relative Tracer Retention (%) Stress	Rest	Absolute Flow (ml/min/g) Stress	Rest	Reserve
LAD	48	77	0.85	0.93	0.91
LCX	73	87	1.40	1.02	1.38
RCA	67	75	1.32	0.95	1.38
Total LV	60	79	1.12	0.94	1.19

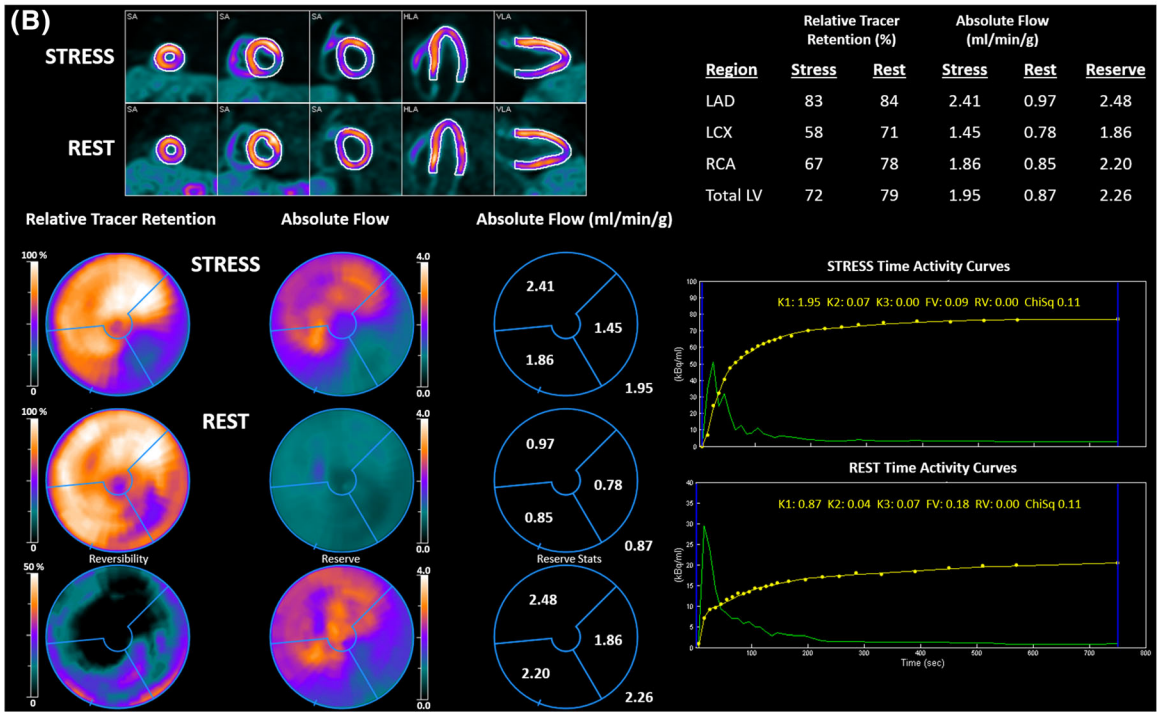

Region	Relative Tracer Retention (%) Stress	Rest	Absolute Flow (ml/min/g) Stress	Rest	Reserve
LAD	83	84	2.41	0.97	2.48
LCX	58	71	1.45	0.78	1.86
RCA	67	78	1.86	0.85	2.20
Total LV	72	79	1.95	0.87	2.26

accuracy. In the present study, we sought to evaluate the incremental diagnostic accuracy of ^{18}F-flurpiridaz flow measurements in the multicenter flurpiridaz 301 trial against quantitative coronary angiography.

METHODS

Study Population

Patients were enrolled in the 301 trial at 81 sites worldwide. Inclusion criteria included men and women ≥ 18 years of age who underwent invasive coronary angiography (ICA) without intervention, clinically indicated myocardial perfusion SPECT, and were capable of undergoing exercise or pharmacologic stress. Major exclusion criteria were unstable cardiovascular status including myocardial infarction within 6 months of ^{18}F-flurpiridaz PET, percutaneous coronary intervention (PCI) or other invasive coronary procedures within 6 months prior to ^{18}F-flurpiridaz PET, history of coronary artery bypass graft surgery, or current non-ischemic cardiomyopathy. Pre-test probability of CAD was determined according to ACC/AHA guidelines for exercise testing.[18] Primary study results and trial design have been previously published.[5] The availability of adequate quality dynamic PET images at rest and pharmacologic stress was an additional inclusion criterion for this secondary analysis which was not prespecified (dynamic imaging was optional at the discretion of the recruiting sites). All patients provided written informed consent prior to undergoing study procedures.

Coronary Angiography

Invasive coronary angiography was performed in accordance with institutional practice at each investigational site, and images were evaluated by a single blinded reader at the angiographic core laboratory (Boston Clinical Research Institute, Boston, MA USA) using quantitative methods (QCA PlusPlus, Sanders Data Systems, Palo Alto, CA USA). Angiographic obstructive disease was defined as either ≥ 50% or ≥ 70% reduction in luminal diameter.

Image Acquisition Protocol

Centralized quality control assessment was performed for each PET scanner prior to use in the 301 trial. A total of nine PET/CT scanner models from three vendors were represented in the present substudy (Supplemental Figure 1). ^{18}F-flurpiridaz PET exams were performed within a median of 2 ± 28 days of ICA. PET preceded ICA in 131 (57%) of patients in this study. All patients were instructed to fast for at least 3 h before the imaging exam. PET imaging was performed on qualified scanners in 2D or 3D mode with CT attenuation correction, except one exam which utilized a rotating transmission source for attenuation correction. Dynamic PET acquisition at rest was initiated with intravenous bolus injection of ^{18}F-flurpiridaz (100 ± 7 MBq) immediately followed by a 5-10 mL saline flush. PET images were acquired

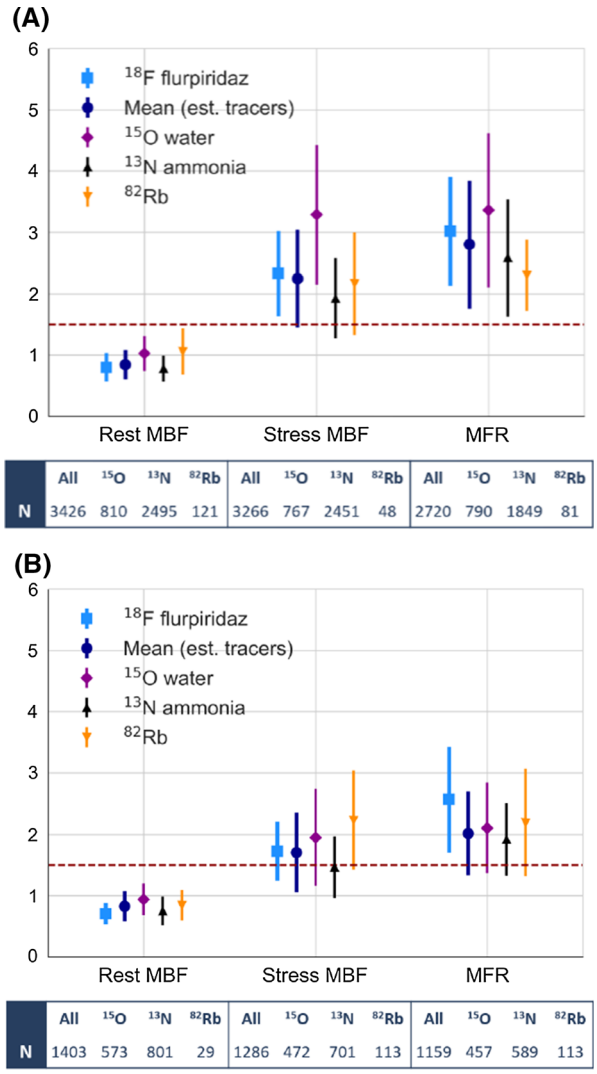

Figure 2. Comparison between absolute flow and flow reserve measured by ^{18}F-flurpiridaz PET and three established PET flow tracers. **A** Patients with risk factors only (N = 131); **B** CAD patients (50% stenosis, N = 100). Other tracer data are from Table 2 of the online appendix to Ref. 37. The number of patients contributing to established tracer data points is shown below the graphs. Mean(est. tracers) indicates weighted mean ± pooled SD of established tracers.

for 15 minutes. After quality control for alignment of PET and attenuation images,[19] PET images were reconstructed with standard PET corrections (attenuation, randoms, scatter, deadtime, decay) without post-smoothing filter, according to prescribed time frames (15 × 10 seconds, 5 × 30 seconds, 5 × 60 seconds, 1 × 300 seconds). Pharmacologic stress was performed with adenosine, dipyridamole, or regadenoson according to local practice and the respective package inserts. At peak stress, dynamic PET image acquisition and reconstruction was repeated with intravenous bolus injection of ^{18}F-flurpiridaz (218 ± 11 MBq). Static images were created by summing the dynamic PET images after the initial 2 minutes.

Table 2. ^{18}F-flurpiridaz flow and flow reserve

Presence of disease	N	Stress MBF	Rest MBF	MFR
No obstructive CAD	121	2.36 ± 0.66	0.81 ± 0.23	3.02 ± 0.90**
1-vessel CAD	53	1.89 ± 0.45†	0.74 ± 0.19‡	2.71 ± 0.85
2- or 3-vessel CAD	30	1.46 ± 0.39†,*	0.69 ± 0.16‡	2.21 ± 0.75†,**

Global left ventricular rest and stress MBF and MFR per patient stratified by presence of disease (N = 204; 50% stenosis threshold; 27 patients were excluded with evidence of infarction on the rest PET scan)
N number of patients per subgroup, *MBF*, myocardial blood flow (mL/min/g); *MFR*, myocardial flow reserve; *CAD*, coronary artery disease
†$P < 0.001$ compared to No CAD
*$P < 0.001$ compared to 1-Vessel CAD
‡$P < 0.05$ compared to No CAD
**$P < 0.05$ compared to 1-Vessel CAD

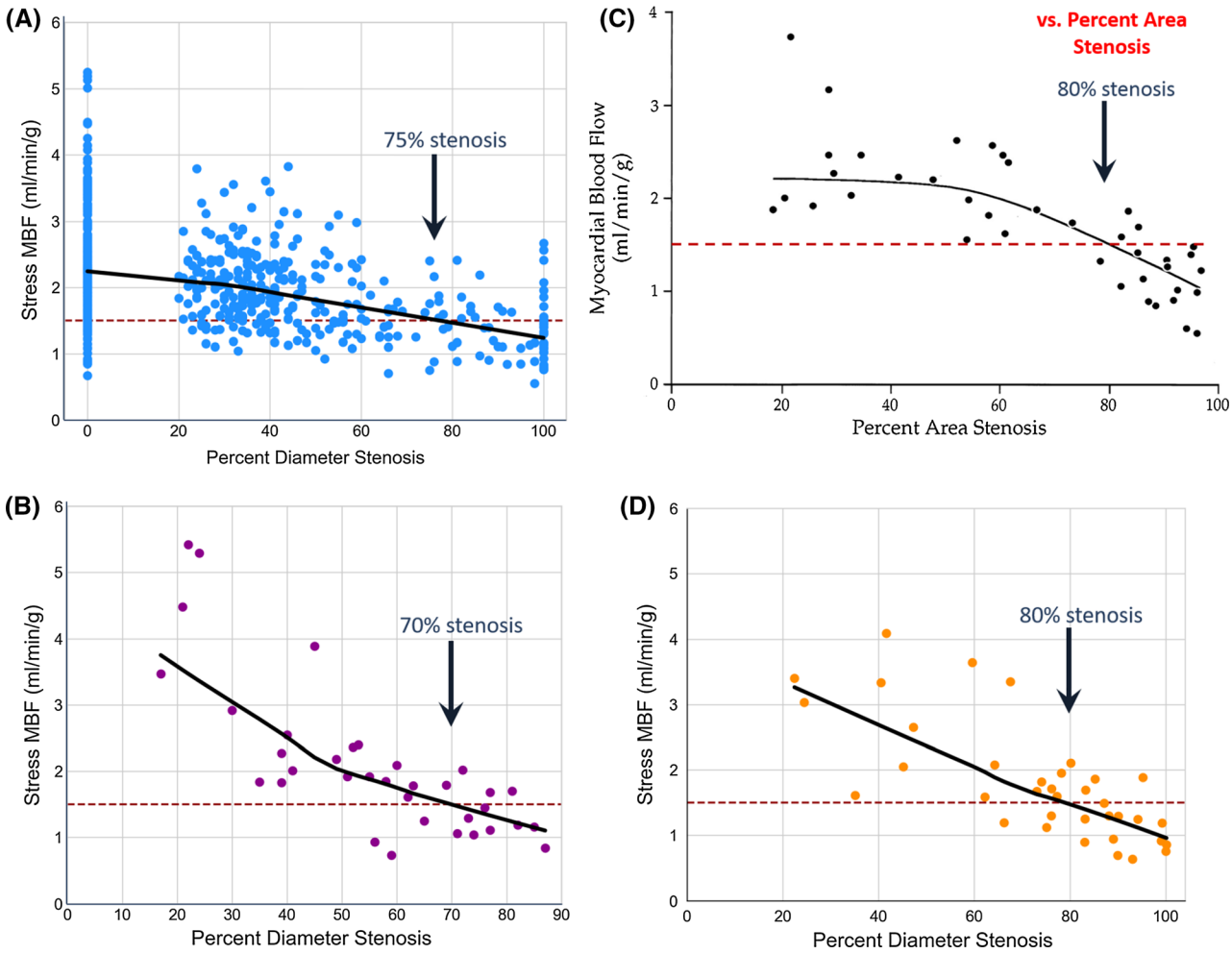

Figure 3. Stress flow versus stenosis severity per vessel. **A** ^{18}F-flurpiridaz PET from the present study, **B** ^{15}O-water PET from Ref. 38, **C** ^{13}N-ammonia PET from Ref. 39, and **D** ^{82}Rb PET from Ref. 40. Solid black curves are non-parametric locally weighted least squares fits representing average flow, and dashed red lines represent a commonly used lower limit of normal stress flow.[41] The crossing point of this lower limit with the average stress flow was between 70 and 80% stenosis for these tracers.

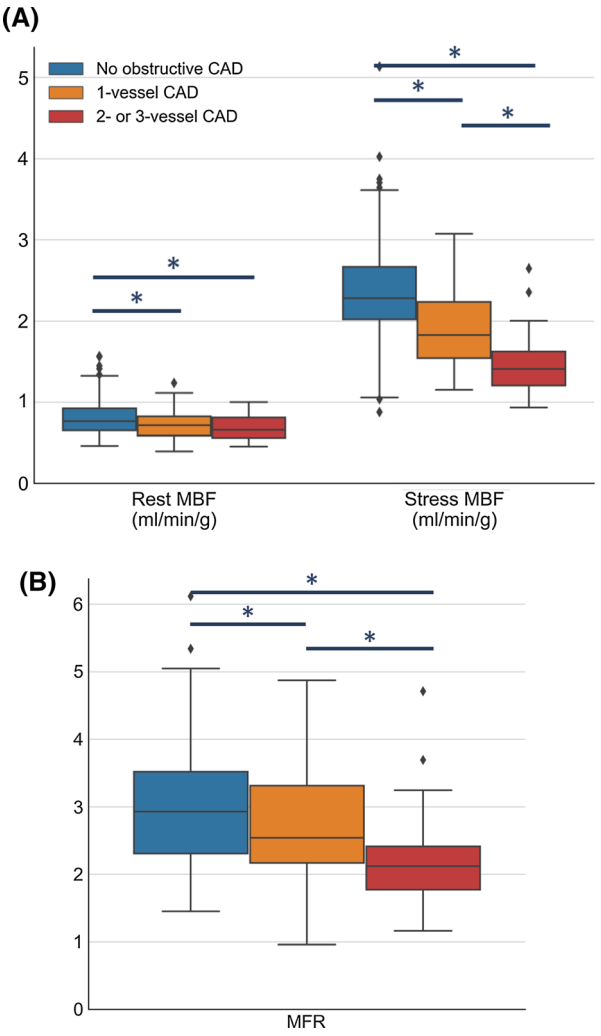

Figure 4. ^{18}F-flurpiridaz flow and flow reserve. Per-patient distributions of global left ventricular rest and stress MBF (**A**) and MFR (**B**) (N= 204 patients; obstructive CAD was defined by a 50% stenosis threshold; 27 patients were excluded with evidence of infarction on the rest PET scan). *$P < 0.05$.

The time between rest and stress ^{18}F-flurpiridaz administration was 52 ± 11 minutes and no shorter than 30 minutes.

Image Analysis

For this secondary analysis, images were processed using Corridor4DM software version 2017 (INVIA Medical Imaging Solutions, Ann Arbor, MI). Static PET images of the heart were transformed to short axis orientation and left ventricular (LV) contours representing the endo- and epicardial boundaries were defined semi-automatically[20] and applied to each dynamic frame. Patient motion between dynamic frames was visually identified and manually corrected.[21]

Relative Tracer Retention Polar maps of relative tracer retention representing relative perfusion were generated from static PET images and normalized to peak ^{18}F-flurpiridaz uptake in the left ventricle. Thirty-two patients without history of previous PCI, MI, stroke, heart failure, or acute coronary syndrome, and without angiographic evidence of coronary artery disease were selected for inclusion in a database to represent normal myocardial ^{18}F-flurpiridaz distribution. The normal database was then used to estimate stress total perfusion deficit (TPD)[22] as a measure of perfusion defect extent and severity in all patients. Vascular territories with evidence of infarction on the rest PET scan (moderate to severe defect corresponding to severity > 5.5 SD using the normal databases) were excluded because MBF and MFR may not be reliably estimated in such regions (N = 37 territories in 27 patients).

Absolute Myocardial Blood Flow PET time-activity curves (TACs) were automatically sampled from 460 regions in the LV myocardium. An image-derived (whole blood) arterial input function was automatically sampled from a 3D region of interest extending from the left atrium into the left ventricle and centered near the mitral valve plane in each dynamic frame.[23,24] Due to the lack of arterial blood samples or validated correction models, no corrections of the input function for metabolites and blood-binding were performed. Residual activity on the stress scan from tracer injection at rest was estimated and subtracted from TACs as previously described[7,8,10] after ensuring proper image registration of the initial dynamic frames before arrival of the tracer bolus to the heart. A 3 × 3 mean filter was applied to dynamic polar maps followed by kinetic modeling using a previously described 2-tissue-compartment (also known as 3-compartment) model that was validated in a porcine model against microsphere flow.[7,8] The influx rate constant K1 was equated with flow since it is equal to flow times extraction fraction, and previous preclinical data demonstrated very high first-pass extraction fraction of 0.94.[25] Polar maps were generated of absolute flow (MBF, in units mL/min/g) and flow reserve (MFR, stress flow divided by rest flow) which are reported as global LV average and per vascular territory.

Statistical Analysis

Continuous variables are reported as mean ± SD unless noted otherwise. Continuous and categorical variables were compared by t tests and χ^2 tests, respectively. For global analysis, patients were stratified by number of vessels with obstructive disease, and for per-vessel analysis, vascular territories were stratified by increasing severity of stenosis with the lowest severity subgroups further divided based on the presence of any remote obstructive CAD. Unadjusted receiver operating characteristic (ROC) curves for detecting obstructive CAD were analyzed with stress MBF or MFR and compared using DeLong's test.[26] ROC thresholds were selected with Youden's index,[27] and differences in sensitivity and specificity, and positive and negative predictive values were tested with McNemar's test[28] and Leisenring's test,[29] respectively. The incremental diagnostic value of MBF and MFR was assessed with multivariable logistic modeling that included patient age, sex, BMI, and pre-test likelihood of CAD as

covariates, as well as stress TPD. Per-vessel logistic mixed modeling with the same covariates was also performed to account for within-patient correlations between vascular territories. Log transformations toward normality were applied to BMI, TPD, stress MBF and MFR.[30] Linearity of predictors and presence of interaction terms were checked by modeling with regression splines[31] and by plotting predictor effects with partial residuals.[32] The change in discrimination after adding stress MBF or MFR to models containing above covariates was assessed with continuous net reclassification improvement (NRI) and the change in concordance index (c-index).[33] Multiple comparisons were performed with an adaptive two-step procedure controlling false discovery rate at a level of 0.05.[34] Two-sided P values < 0.05 were considered significant. Statistical analysis was performed using R version 3.6.1[35] and python version 3.6.5.[36]

RESULTS

Patient Population

A total of 755 patients were recruited for the flurpiridaz 301 trial, of which 559 underwent pharmacologic stress PET. Within this subset, dynamic ^{18}F-flurpiridaz PET data, as provided by GE Healthcare, were available for 276 patients from 43 clinical imaging sites. After quality control for dynamic PET, 231 of these PET exams (84%) were suitable for evaluation in this post hoc flow study. Reasons for quality control failure included: missing or corrupted dynamic images (N = 8); missed LV first-pass during dynamic scan (N = 12); and scaling errors in the early dynamic frames (N = 25). Patient characteristics of the flow subgroup are shown in Table 1, and were not significantly different compared to the entire 301 trial population (Supplemental Table 1). Patients with CAD ($\geq$ 50% stenosis) were older, predominantly men, with significantly higher incidence of hypercholesterolemia, diabetes, history of MI and previous PCI. Two case examples are shown in Figure 1.

Relationship Between Stenosis Severity, Flow, and Flow Reserve

Because reference standard flow values were not available in this retrospective study, we compared our flow estimates to values in the literature. Figure 2 compares ^{18}F-flurpiridaz flow estimates with weighted averages of three cardiac flow tracers (^{13}N-ammonia, ^{15}O-water, and ^{82}Rb) from an extensive literature review that included approximately 15,000 patients in 250 publications (see Table 2 in the online appendix to Ref. 37). For patients with risk factors only (Figure 2A) and patients with CAD (Figure 2B), the average agreement was very good in general, although the average ^{18}F-flurpiridaz flow reserve for CAD patients tended to be somewhat higher than that of other tracers likely due to slightly lower average rest flow (Figure 2B). In Figure 3, the relationship of stress flow to stenosis severity is compared between ^{18}F-flurpiridaz, ^{15}O-water,[38] ^{13}N-ammonia,[39] and ^{82}Rb.[40] Although the data scatter is large, the degree of stenosis at which the average stress flow was equal to a commonly used lower limit of normal stress flow[41] was similar for all four tracers (70-80%).

On a per-patient basis, there was a significant, progressive decline in ^{18}F-flurpiridaz stress flow with increasing extent of disease (Table 2, Figure 4A). Flow reserve exhibited a somewhat flatter response with less dependence on disease extent, although differences between subgroups were statistically significant

Table 3. ^{18}F-flurpiridaz flow and flow reserve

Stenosis severity	N	Stress MBF‡	Rest MBF	MFR**
0-19% (Remote < 50%)	159	2.51 ± 0.80	0.86 ± 0.26	3.04 ± 1.00
20-49% (Remote < 50%)	222	2.24 ± 0.64	0.77 ± 0.22†	3.03 ± 0.90
0-49% (Remote ≥ 50%)	148	1.92 ± 0.49	0.73 ± 0.18†,*	2.75 ± 0.87
50-69%	56	1.72 ± 0.52	0.68 ± 0.18†	2.69 ± 0.95
70-89%	28	1.51 ± 0.45	0.72 ± 0.16†	2.16 ± 0.70
90-100%	43	1.32 ± 0.49	0.71 ± 0.20†	1.97 ± 0.82

Regional left ventricular rest and stress MBF and MFR per vessel stratified by stenosis severity (N= 656; 37 vessels were excluded with evidence of infarction on the rest PET scan)
N number of vascular territories per subgroup, *MBF* myocardial blood flow (mL/min/g), *MFR* myocardial flow reserve
†$P < 0.01$ compared to 0-19%
*$P < 0.01$ compared to 20-49%
‡$P < 0.05$, all pairwise comparisons
**$P < 0.01$, all pairwise comparisons except 0-19% vs 20-49%; 0-49% vs 50-69%; and 70-89% vs 90-100%

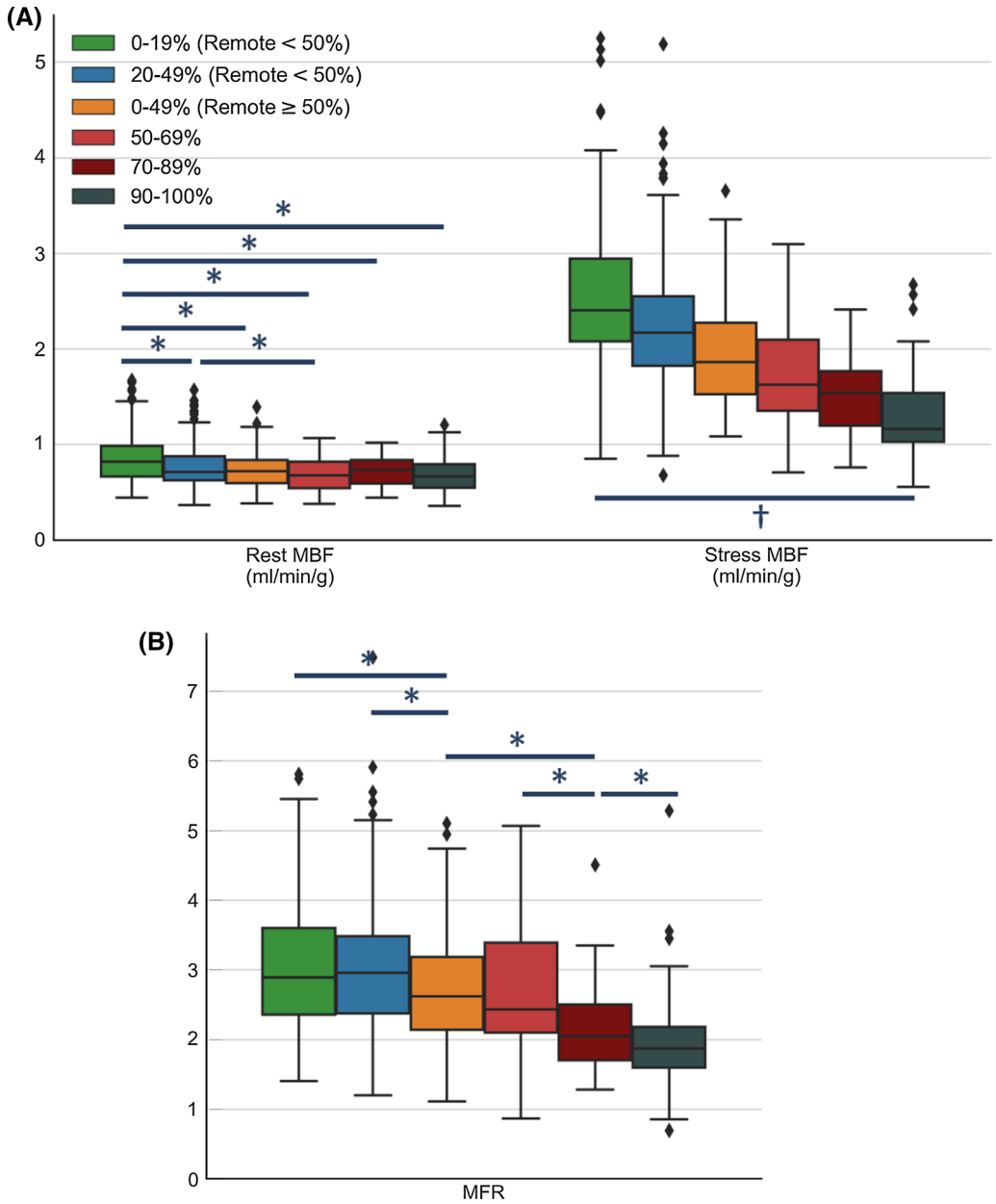

Figure 5. ^{18}F-flurpiridaz flow and flow reserve. Per-vessel distributions of regional rest and stress MBF (**A**) and MFR (**B**) stratified by stenosis severity (N = 656 territories; 37 vessels were excluded with evidence of infarction on the rest PET scan). *$P < 0.05$. †$P < 0.05$, all pairwise differences.

(Figure 4B). In the regional analysis, there was also a progressive decline in stress flow with increasing %stenosis, and again the flow reserve was less dependent on %stenosis (Table 3, Figure 5). When stratified by patient gender, rest and stress flows were significantly higher in women than men ($P < 0.05$), and within-gender differences between the first two vascular subgroups (0-19% and 20-49%) were no longer significant (Supplemental Figure 2).

Diagnostic Performance of Flow and Flow Reserve

In per-vessel unadjusted ROC analysis using a 50% stenosis threshold, the c-index, sensitivity, and NPV were significantly higher for stress flow compared with flow reserve (0.79 vs 0.71, $P < 0.001$; 77 vs 62%, $P < 0.001$; 93 vs 89%, $P < 0.001$) (Figure 6A, Table 4). When a 70% stenosis threshold was used, c-index increased for both flow and MFR but the

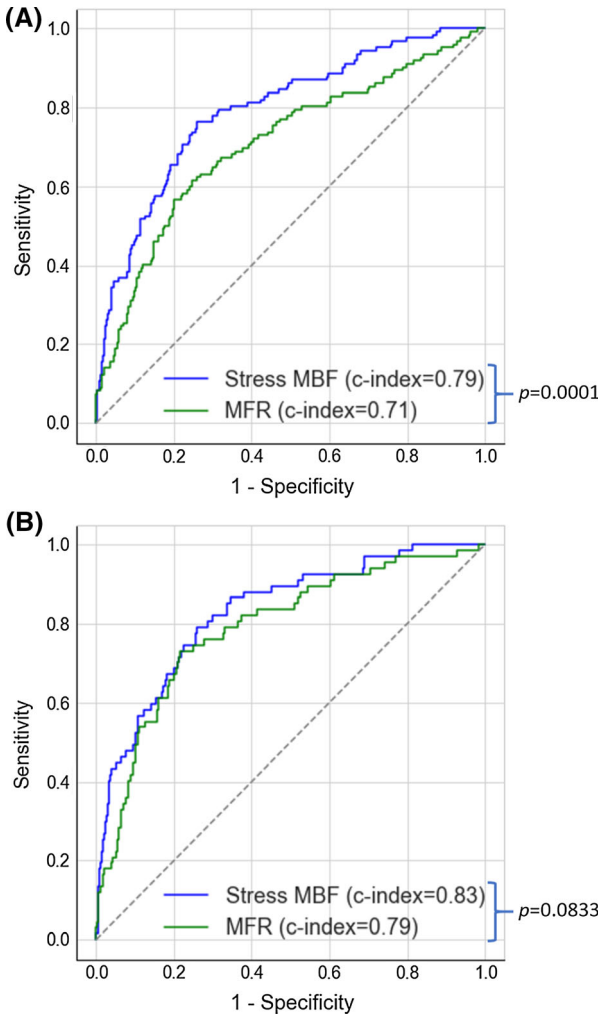

Figure 6. Unadjusted ROC analysis of per-vessel CAD diagnosis with stress MBF or MFR. **A** 50% stenosis threshold and **B** 70% stenosis threshold.

difference was no longer significant (0.83 vs 0.79, $P = 0.0833$) (Figure 6B). However, the specificity of flow reserve was slightly higher than that of stress flow without a significant difference in sensitivity (78 vs 74%, $P = 0.016$; 75 vs 80%, $P = 0.248$, respectively) (Table 4).

Incremental Diagnostic Value of Flow and Flow Reserve

Four multivariable logistic models were tested for the detection of 70% stenosis. On a per-vessel basis, the incremental value of adding stress TPD, MBF, and MFR on accuracy is shown in Table 5. Both stress MBF and TPD (Table 5, Model 3; Figure 7A) and MFR and TPD (Table 5, Model 4; Figure 7B) were significant independent predictors of a 70% stenosis. Models which included all three variables or stress MBF and MFR without TPD (not shown) did not significantly improve model fit, or increase global χ^2 or c-index. After adjustment for clinical covariates and TPD, the c-index of stress MBF and of MFR were not significantly different at 70% stenosis (Figure 7, 0.874 vs 0.869, $P = 0.658$), and marginally different at 50% stenosis (Supplemental Figure 3, 0.825 vs 0.799, $P = 0.043$). Similar features were observed for per-patient models of 70% stenosis (Table 6), and 50% stenosis (Supplemental Tables 2, 3, Supplemental Figs. 3-5). Significant interactions were present in all per-vessel models between stress MBF and TPD and between MFR and TPD, such that the importance of low stress MBF or MFR increased with larger and more severe defects (Figure 8, Supplemental Figure 6). There was no statistical evidence of non-linearity for either MBF or MFR. Overall NRI (Table 7) ranged from 0.219 to 0.559 and was significantly greater than zero ($P < 0.05$) in all but one model (MFR, per patient with 70% threshold, Supplemental Table 4). The improvement in c-index after adding stress MBF or MFR to per-vessel base models plus TPD ranged from 0.006 to 0.043, and was significant for stress MBF at 50% stenosis threshold ($P < 0.05$) (Table 7).

DISCUSSION

The results of this retrospective analysis of 276 patients from the multicenter flurpiridaz 301 trial demonstrate that global and regional ^{18}F-flurpiridaz absolute flow and flow reserve may provide incremental diagnostic value for detecting obstructive CAD. Previous studies have shown similar results for absolute MBF and MFR derived from ^{13}N-ammonia,[11–13] ^{82}Rb,[16,17] and ^{15}O-water [14,15] cardiac PET. All of these were single-center studies except that of Danad et al.[15] which included three highly experienced academic PET centers. Importantly, the present multicenter study included PET data acquired at 43 clinical sites, including many smaller non-academic outpatient imaging centers, and used nine different PET/CT scanner models from three vendors (Supplemental Figure 1), supporting methodologic robustness in clinical practice.

Diagnostic Value of Stress MBF and MFR

In ROC analysis (Figure 6, Table 4), stress MBF provided more accurate detection of CAD than MFR, although this comparison was not adjusted for clinical covariates known to be associated with increased likelihood of CAD. In our study population, patients with obstructive CAD were more likely to be men and those greater than 60 y of age. In addition, both age and sex

Table 4. Unadjusted diagnostic performance of ^{18}F-flurpiridaz stress MBF and MFR for detecting angiographic CAD (see Figure 6)

	Sensitivity	Specificity	PPV	NPV
50% stenosis, per patient				
Stress MBF	73	75*	67*	81
MFR	72	59	55	76
50% stenosis, per vessel				
Stress MBF	77†	74	41	93†
MFR	62	75	37	89
70% stenosis, per patient				
Stress MBF	77	76	52	91
MFR	63	72	44	85
70% stenosis, per vessel				
Stress MBF	80	74	27	97
MFR	75	78*	29	96

†$P < 0.001$, stress MBF compared to MFR
*$P < 0.05$, stress MBF compared to MFR

were more strongly correlated with stress MBF than MFR (multiple R^2 0.272 vs 0.029, both $P < 0.0001$) such that women and younger patients had significantly higher stress MBF. Thus, without adjustment for age and sex, stress MBF would appear to have a diagnostic advantage over MFR based largely on patient demographics. After adjusting for these covariates in our logistic models, stress MBF and MFR performed similarly in terms of overall c-index (0.874 vs 0.869, $P = 0.658$) (Figure 7; see also Supplemental Figs. 3-5).

In contrast, MFR in the context of *prognostic* assessment has consistently been a stronger predictor of cardiovascular mortality than stress MBF when adjusted for age, sex, LV ejection fraction, and the extent and severity of ischemia and scar[42,43] (see also Ref. 44 which did not meet these conditions). In this case, MFR can be reduced by additional factors not directly related to likelihood of obstructive epicardial CAD, such as resting hyperemia due to increased rate-pressure product, decreased myocardial efficiency, or autonomic dysfunction.[45,46]

Anatomical assessment by ICA correlates poorly with the hemodynamic functional significance of epicardial stenosis.[41] Recent studies[14,15] that have defined functional significance by invasive fractional flow reserve (FFR) have tended to report higher unadjusted diagnostic accuracy for stress MBF and MFR (e.g., c-index from 0.84 to 0.94) than the present study (c-index from 0.71 to 0.83, Figure 6). This may reflect the limitations of using solely an anatomical definition of obstructive CAD (as in the present study), as opposed to more contemporary functional definitions.[37]

Comparison with Established Flow Tracers

The comparison of ^{18}F-flurpiridaz with other tracers illustrates two important points about flow variability and abnormal thresholds. First, for a given tracer, stress flow is widely scattered, particularly for non-obstructive stenoses < 50% (Figure 3). This variability is due to physiological differences in the integrated tissue response to hyperemia as measured by PET, which may be affected by patient age,[47] sex,[48,49] variations in pharmacologic vasodilation responsiveness,[38] and varying degrees of subclinical atherosclerosis and microvascular dysfunction.[37] Flow variability between tracers (Figure 2) arises from well-known physical differences in tracer characteristics. The first-pass extraction fraction of ^{15}O-water, which is freely diffusible, is independent of flow, whereas that of retained tracers typically decreases non-linearly with increasing flow.[50] Although established tracers have often been validated against microspheres or ^{15}O-water flow in carefully controlled animal studies (see[50] for references), most flow models of retained tracers require empirical extraction correction which may introduce characteristic flow differences when applied to clinical patient populations.[51] Such absolute flow differences are most noticeable under hyperemic conditions and are progressively less important under resting or low flow conditions (Figure 2).

Second, the stress MBF threshold of 1.5 mL/min/g shown in the figures has been recommended as a lower limit of ''definitely abnormal'' flow, but is not intended to represent an optimal threshold of obstructive CAD common to all flow tracers.[41] While this threshold

Table 5. Per-vessel multivariable logistic mixed models for detection of 70% stenosis demonstrating incremental diagnostic value of stress TPD, stress MBF, and MFR (N = 656)

	Model 1		Model 2		Model 3		Model 4	
Fit Statistic	**Estimate[b]**	***P***	**Estimate[b]**	***P***	**Estimate[b]**	***P***	**Estimate[b]**	***P***
Global χ^2 [df][a]	19.0 [7]	Referent	110.8 [8]	< 0.0001	153.3 [10]	< 0.0001	143.6 [10]	< 0.0001
AIC	434	-	344	-	306	-	316	-
c-index	0.673	Referent	0.863	< 0.0001	0.874	0.369	0.869	0.548
Variable								
Intercept	− 1.09 (3.91)	0.780	− 4.75 (4.35)	0.275	3.28 (5.33)	0.538	− 5.71 (5.45)	0.295
Age	0.32 (0.17)	0.058	0.37 (0.19)	0.049	0.11 (0.21)	0.609	0.27 (0.22)	0.225
Male sex	1.09 (0.43)	0.011	0.67 (0.49)	0.174	− 0.36 (0.59)	0.548	1.03 (0.61)	0.091
Log(BMI)	− 0.38 (1.09)	0.727	0.38 (1.19)	0.750	− 1.03 (1.42)	0.470	0.79 (1.46)	0.588
Pre-test likelihood of CAD								
Intermediate (10-90%)	− 1.40 (0.50)	0.005	− 0.88 (0.55)	0.108	− 0.82 (0.64)	0.204	− 0.76 (0.67)	0.251
High (> 90%)	− 1.03 (0.49)	0.035	− 1.23 (0.53)	0.021	− 1.04 (0.63)	0.098	− 1.21 (0.65)	0.065
Log(stress TPD)			0.77 (0.12)	< 0.0001	1.08 (0.33)	0.0009	1.33 (0.34)	0.0001
Log(stress MBF)					− 3.49 (1.34)	0.009		
Log(stress TPD) × log(stress MBF)					− 0.89 (0.41)	0.029		
Log(MFR)							− 1.23 (1.01)	0.226
Log(stress TPD) × log(MFR)							− 0.77 (0.31)	0.012

[a]Global likelihood ratio χ^2 and c-index are for entire models with df degrees of freedom; AIC indicates Akaike Information Criterion; Fit statistic *P* values compare Models 2 - 1, Models 3 - 2, and Models 4 - 2, respectively. The difference in c-index between Models 3 and 4 was not significant (*P* = 0.658)
[b]Coefficient standard errors are given in parentheses

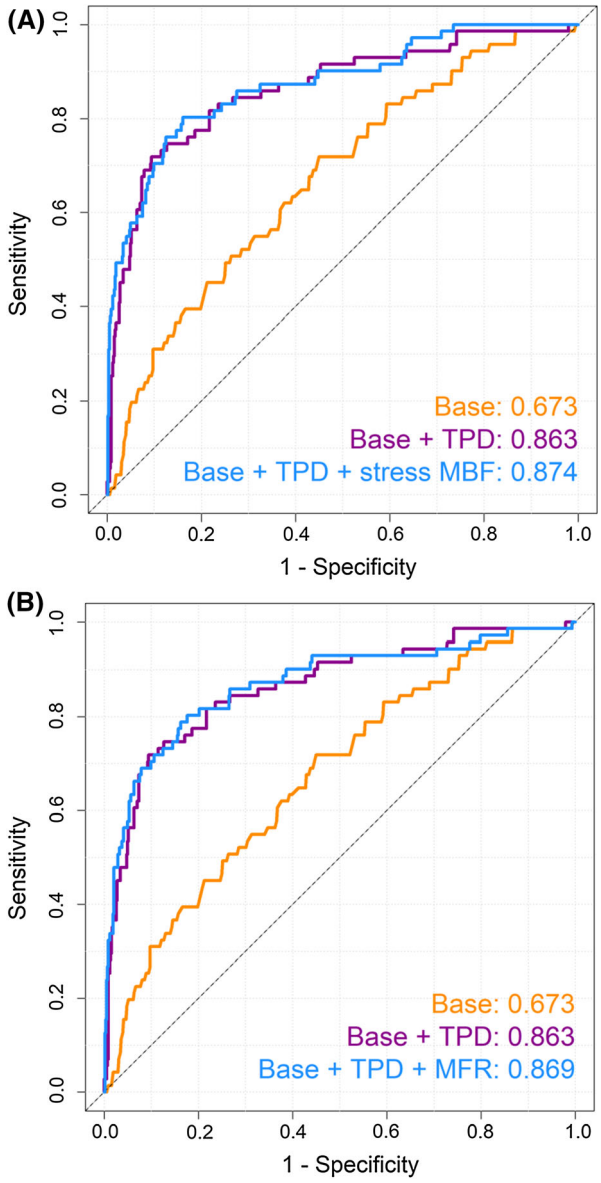

Figure 7. Adjusted ROC analysis of per-vessel CAD diagnosis (70% stenosis threshold) with stress MBF (**A**) (Table 5) and MFR (**B**) (Table 6). Base models included patient age, sex, BMI, and pre-test likelihood of CAD. Figure legends indicate c-index values for each nested model.

indicates a similar *average* stenosis severity (70-80%), there is considerable scatter around this average behavior for all four tracers (Figure 3). Optimal thresholds of significant CAD will generally vary according to tracer characteristics, kinetic modeling methodology (e.g., Supplemental Figure 7), and the definition of obstructive CAD.[41] For example, stress MBF thresholds of 1.86,[52] 2.30,[15] and 2.50[14,53] have recently been proposed for ^{15}O-water, depending on the choice of stenosis threshold, methodologic variations, and whether the definition of obstructive CAD included functional assessment by FFR.

Although ^{18}F-flurpiridaz stress flow in this study followed an inverse relationship with stenosis severity that was similar to other tracers,[38–40] we also observed significantly higher rest flow in the lowest severity subgroup (0-19% stenosis) compared to the other subgroups (Figure 5A) which seems to conflict with previous findings.[38–40] This may be a consequence of significantly higher rest flow in women compared to men in the present study (Supplemental Figure 2), and the fact that women contributed nearly two-thirds (100/159) of vessels in the lowest subgroup, but just 21% (102/497) in all other subgroups combined. Similarly, stress flow was significantly higher in women compared to men in the 3 least severe subgroups, although the corresponding flow reserves did not differ significantly (Supplemental Figure 2), in agreement with previous ^{15}O-water,[49] ^{13}N-ammonia,[48] and ^{82}Rb[45,46] PET studies.

^{18}F-flurpiridaz Kinetic Model

In this study, we used a 2-tissue-compartment kinetic model previously validated for ^{18}F-flurpiridaz against microsphere flow in pigs.[7,8] A prior single-center study of 15 patients,[10] which used a novel kinetic model without validation, reported flow estimates generally similar to ours (Table 8), although both studies lacked reference standard flow measurements.

The accuracy of ^{18}F-flurpiridaz flow measurement can potentially be affected by several factors. Substantial residual activity was present during the stress scan which followed the rest scan by 52 ± 11 minutes (approximately 0.5 × ^{18}F half-life). Similar ^{18}F-flurpiridaz protocols have been reported in previous human and animal studies.[7,8,10] Stress flow accuracy depends on correcting this residual activity, and these studies have used the simplest approach of estimating residual activity in the early dynamic frames before tracer arrival to the left ventricle and direct subtraction of this estimate from the time-activity curves. Although straightforward, this residual correction can be adversely affected by patient motion and poor count density in the early frames, and more sophisticated modeling approaches have been proposed.[9]

Another important factor is the use of an image-derived whole blood arterial input function which assumes rapid tracer equilibration between plasma and red blood cells with negligible blood-binding or tracer metabolism. However, in previous ^{18}F-flurpiridaz animal studies, Guehl et al.[9] described a blood-binding correction of the input function, while other authors have discussed the potential need for metabolite correction.[7,10] Without correction, either of these processes

Table 6. Per-patient multivariable logistic models for detection of 70% stenosis demonstrating incremental diagnostic value of stress TPD, stress MBF, and MFR (N = 204)

	Model 1		Model 2		Model 3		Model 4	
Fit Statistic	**Estimate[b]**	***P***	**Estimate[b]**	***P***	**Estimate[b]**	***P***	**Estimate[b]**	***P***
Global χ^2 [df][a]	21.3 [6]	Referent	77.7 [7]	<0.0001	91.9 [8]	0.0002	82.9 [8]	0.023
AIC	222	-	168	-	156	-	165	-
c-index	0.708	Referent	0.878	< 0.0001	0.896	0.182	0.882	0.730
Variable								
Intercept	− 0.14 (4.18)	0.973	− 5.21 (4.96)	0.294	1.49 (5.58)	0.789	− 2.98 (5.21)	0.568
Age	0.30 (0.18)	0.091	0.38 (0.20)	0.059	0.15 (0.22)	0.485	0.30 (0.21)	0.150
Male sex	1.23 (0.45)	0.006	0.73 (0.53)	0.166	0.01 (0.61)	0.987	0.81 (0.55)	0.140
Log(BMI)	− 0.24 (1.17)	0.838	0.68 (1.34)	0.614	− 0.18 (1.46)	0.902	0.46 (1.39)	0.744
Pre-test likelihood of CAD								
Intermediate (10-90%)	− 1.56 (0.56)	0.005	− 0.94 (0.67)	0.157	− 0.91 (0.71)	0.205	− 0.87 (0.69)	0.203
High (> 90%)	− 0.83 (0.54)	0.127	− 1.10 (0.64)	0.084	− 0.92 (0.69)	0.183	− 1.03 (0.66)	0.118
Log(stress TPD)			0.77 (0.12)	< 0.0001	0.87 (0.20)	< 0.0001	0.97 (0.21)	< 0.0001
Log(stress MBF)					− 3.93 (1.12)	0.0005		
Log(MFR)							− 1.49 (0.68)	0.028

[a]Global likelihood ratio χ^2 and c-index are for entire models with df degrees of freedom; AIC indicates Akaike Information Criterion; Fit statistic *P* values compare Models 2 - 1, Models 3 - 2, and Models 4 - 2, respectively. The difference in c-index between Models 3 and 4 was not significant (*P* = 0.107)
[b]Coefficient standard errors are given in parentheses

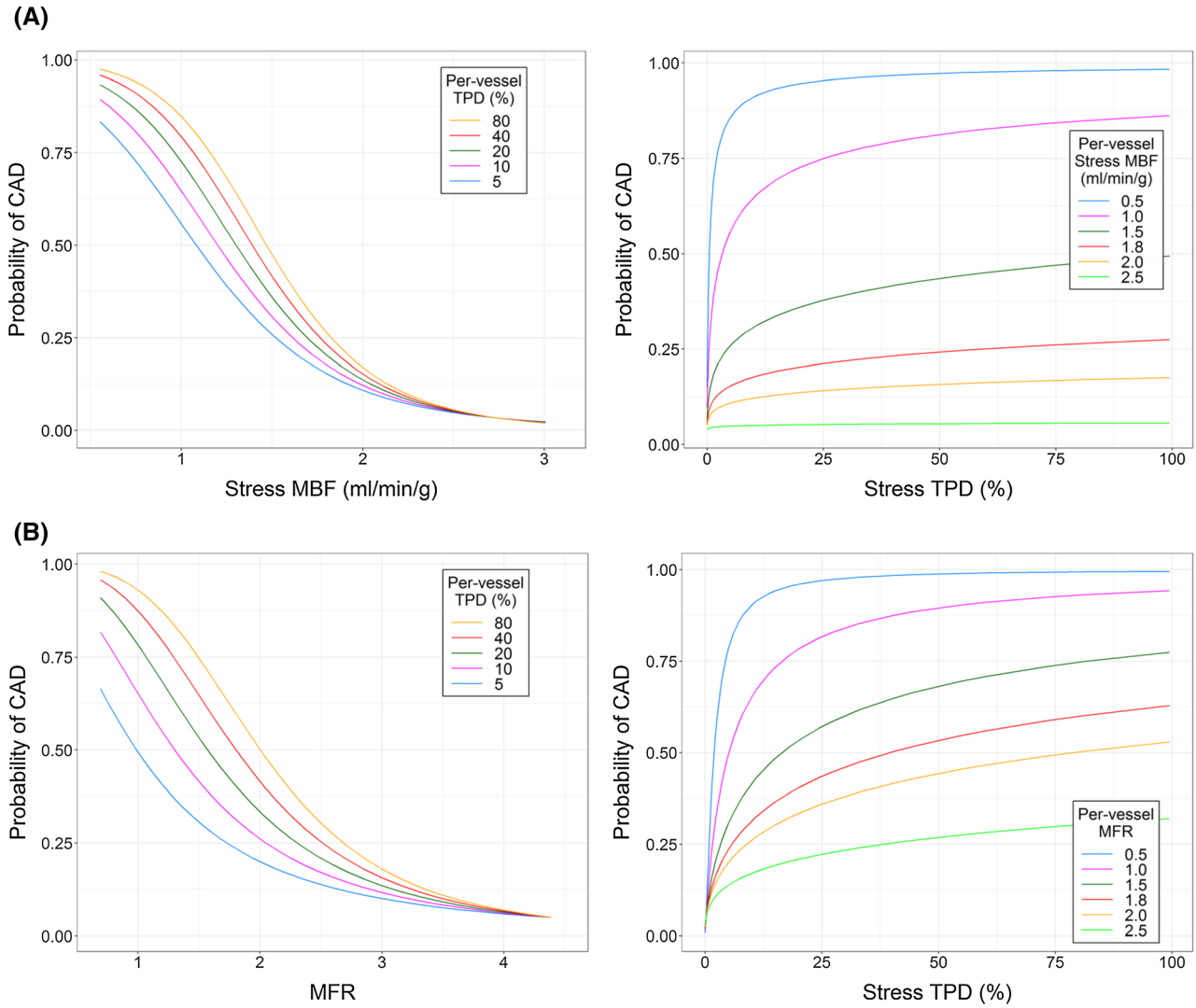

Figure 8. Per-vessel interactions for the logistic models in Table 5 (70% stenosis threshold). **A** Model 3, between stress MBF (left) and TPD (right); and **B** Model 4, between MFR (left) and TPD (right).

could cause overestimation of the plasma input function, which in turn would result in flow underestimation. In fact, Nekolla et al.[7] observed a modest underestimation of flow without metabolite correction, particularly in ischemic regions, while Guehl et al.[9] did not observe any bias after blood-binding correction. Although these factors have yet to be fully characterized in humans, our results seem to indicate that their contribution to flow variations is relatively minor.

STUDY LIMITATIONS

This study had several limitations. First, only about half (276/559) of the pharmacologic stress PET data sets acquired in the 301 trial were available for analysis. This limited the number of available diseased vessels in women (Supplemental Figure 2), and likely limited the statistical power of ROC analysis and logistic regression modeling. Second, detailed anatomical information beyond stenosis severity from invasive coronary angiography was not available, precluding assessment of coronary dominance which could confound the evaluation of left circumflex and right coronary artery territories. Third, the acquisition protocol in the 301 trial was suboptimal for estimating residual activity in

Table 7. Continuous net reclassification improvement (NRI) of logistic regression models of CAD detection after including stress MBF or MFR

Covariate added to Base + TPD model	Overall NRI	NRI (CAD)	NRI (no CAD)	Δ c-index
50% stenosis				
Stress MBF, per patient	0.559† [0.279, 0.830]	0.253† [0.041, 0.459]	0.306† [0.134, 0.479]	0.021
Stress MBF, per vessel	0.412† [0.236, 0.573]	0.433† [0.285, 0.583]	− 0.021 [− 0.104, 0.063]	0.043†
MFR, per patient	0.288† [0.015, 0.556]	0.181 [− 0.034, 0.387]	0.107 [− 0.069, 0.280]	0.003
MFR, per vessel	0.342† [0.142, 0.535]	0.181† [0.008, 0.354]	0.161† [0.074, 0.250]	0.017
70% stenosis				
Stress MBF, per patient	0.413† [0.104, 0.715]	0.308† [0.041, 0.560]	0.105 [− 0.052, 0.267]	0.018
Stress MBF, per vessel	0.286† [0.029, 0.503]	0.380† [0.139, 0.583]	− 0.094† [− 0.178, − 0.008]	0.011
MFR, per patient	0.219 [− 0.099, 0.523]	0.192 [− 0.083, 0.461]	0.026 [− 0.134, 0.187]	0.004
MFR, per vessel	0.285† [0.037, 0.532]	0.099 [− 0.141, 0.333]	0.186† [0.104, 0.266]	0.006

Base models included patient age, sex, BMI, and pre-test likelihood of CAD. NRI(CAD) and NRI(no CAD) indicate NRI estimates for patients with and without angiographic (obstructive) CAD, respectively, and overall NRI is their sum. Bracketed intervals are bootstrap 95% confidence intervals. Δ c-index indicates the change in c-index after adding stress MBF or MFR to the Base + TPD model

†$P < 0.05$, testing the null hypotheses NRI = 0 or Δ c-index = 0

Table 8. Comparison of ^{18}F-flurpiridaz flow and flow reserve per vessel in patients

Patients	N	Stress MBF	Rest MBF	MFR
Packard et al.[10]				
Low likelihood patients†	21	2.55 ± 0.54	0.73 ± 0.14	3.73 ± 0.57
CAD patients (< 50% stenosis)	12	2.02 ± 0.40	0.73 ± 0.09	2.97 ± 0.76
CAD patients (≥ 50% stenosis)	12	1.43 ± 0.31	0.86 ± 0.21	1.86 ± 0.59
Current study				
Patients without CAD	381	2.35 ± 0.71	0.81 ± 0.24	3.03 ± 0.94
CAD patients (< 50% stenosis)	148	1.92 ± 0.49	0.68 ± 0.18	2.69 ± 0.95
CAD patients (≥ 50% stenosis)	127	1.54 ± 0.50	0.70 ± 0.18	2.33 ± 0.86

N number of vascular territories per subgroup, *MBF* myocardial blood flow (mL/min/g), *MFR* myocardial flow reserve, *CAD* coronary artery disease

†Low likelihood values shown here are weighted averages of per-vessel values in Table 1 of ref 10

the stress images which, in many cases, consisted of a single 10-second frame. The residual correction could be improved by acquiring at least 30 seconds of list-mode data prior to initiating pharmacologic stress and tracer administration. Fourth, as mentioned previously, the study lacked reference standard flow measurements which will be necessary in the future to validate appropriate ^{18}F-flurpiridaz kinetic models in humans. Finally, the 32 low-risk patients used to define normal databases of myocardial ^{18}F-flurpiridaz retention were also included in the multivariable logistic regression models, which could potentially overstate the performance of TPD in these models compared to using an externally defined normal database. However, the

magnitude of such an effect is small, and would not affect our conclusions regarding the performance MBF or MFR (see Supplemental Table 4).

CONCLUSION

We have characterized ^{18}F-flurpiridaz flow and flow reserve in a large multicenter patient population with invasive coronary angiographic correlates. Both stress flow and flow reserve per vessel were inversely related to stenosis severity, generally agreed with average values from the extensive literature on other flow tracers, and added incremental diagnostic value beyond clinical characteristics and relative perfusion analysis. ^{18}F-flurpiridaz PET shows promise for routine application of clinical flow quantification.

NEW KNOWLEDGE GAINED

^{18}F-flurpiridaz is an investigational radiotracer for PET myocardial perfusion. Using data from the international multicenter phase 3 flurpiridaz 301 trial, we report the first study demonstrating the added diagnostic value of absolute myocardial blood flow (MBF) and flow reserve (MFR) beyond traditional relative perfusion imaging. We show that both stress MBF and MFR meaningfully improve non-invasive diagnosis of obstructive coronary disease identified on invasive coronary angiography.

Acknowledgements

The authors thank Felicia Friend for assistance with data collection, and Francois Tranquart and Matt Morrison for helpful discussions.

Disclosure

J.B. Moody, A. Poitrasson-Rivière, and T. Hagio are employees of INVIA. R.L. Weinberg has nothing to declare. E.P. Ficaro and J.R. Corbett are stockholders of INVIA, which produces 4DM, a clinical software package for cardiac PET analysis. V.L. Murthy declares research support from INVIA. He has received research grants and speaking honoraria from Siemens Medical Imaging. He has served as an advisor to Covidien and Ionetix. He has provided expert witness testimony on behalf of Jubilant DraxImage. He owns stock General Electric and Cardinal Health and stock options in Ionetix.

References

1. Maddahi J, Czernin J, Lazewatsky J, et al. Phase I, first-in-human study of BMS-747158, a novel ^{18}F-labeled tracer for myocardial perfusion PET: Dosimetry, biodistribution, safety, and imaging characteristics after a single injection at rest. J Nucl Med 2011;52:1490-8.
2. Berman DS, Maddahi J, Tamarappoo BK, et al. Phase II safety and clinical comparison with single-photon emission computed tomography myocardial perfusion imaging for detection of coronary artery disease: Flurpiridaz F 18 positron emission tomography. J Am Coll Cardiol 2013;61(4):469-77.
3. Yu M, Nekolla SG, Schwaiger M, Robinson SP. The next generation of cardiac positron emission tomography imaging agents: Discovery of flurpiridaz F-18 for detection of coronary disease. Semin Nucl Med 2011;41:305-13.
4. ClinicalTrials.gov. Bethesda (MD) National Library of Medicine (US) 2000 NLM identifier: NCT01347710. A Phase 3 Multi-center Study to Assess PET Imaging of Flurpiridaz F 18 Injection in Patients With CAD; 2016-Apr-5. https://clinicaltrials.gov/ct2/show/NCT01347710. Accessed 4 Jul 2019
5. Maddahi J, Lazewatsky J, Udelson JE, et al. The first phase 3 international multicenter clinical trial of flurpiridaz F 18 PET myocardial perfusion imaging for evaluation of coronary artery disease. JACC 2020 (in press)
6. ClinicalTrials.gov. Bethesda (MD) National Library of Medicine (US) (2000) NLM identifier: NCT03354273. An International Study to Evaluate Diagnostic Efficacy of Flurpiridaz (18F) Injection PET MPI in the Detection of Coronary Artery Disease (CAD); 2019-Mar-7. https://clinicaltrials.gov/ct2/show/NCT03354273. Accessed 4 Jul 2019.
7. Nekolla SG, Reder S, Saraste A, et al. Evaluation of the novel myocardial perfusion positron-emission tomography tracer ^{18}F-BMS-747158-02: Comparison to ^{13}N-ammonia and validation with microspheres in a pig model. Circulation 2009;119:2333-42.
8. Sherif HM, Nekolla SG, Saraste A, et al. Simplified quantification of myocardial flow reserve with flurpiridaz F 18: Validation with microspheres in a pig model. J Nucl Med 2011;52:617-24.
9. Guehl NJ, Normandin MD, Wooten DW, et al. Single-scan rest/stress imaging: Validation in a porcine model with ^{18}F-flurpiridaz. Eur J Nucl Med Mol Imaging 2017;44:1538-46.
10. Packard RRS, Huang S-C, Dahlbom M, Czernin J, Maddahi J. Absolute quantitation of myocardial blood flow in human subjects with or without myocardial ischemia using dynamic flurpiridaz F 18 PET. J Nucl Med 2014;55:1438-44.
11. Muzik O, Duvernoy C, Beanlands R, et al. Assessment of diagnostic performance of quantitative flow measurements in normal subjects and patients with angiographically documented coronary artery disease by means of nitrogen-13 ammonia and positron emission tomography. J Am Coll Cardiol 1998;31:534-40.
12. Hajjiri MM, Leavitt MB, Zheng H, Spooner AE, Fischman AJ, Gewirtz H. Comparison of positron emission tomography measurement of adenosine-stimulated absolute myocardial blood flow versus relative myocardial tracer content for physiological assessment of coronary artery stenosis severity and location. J Am Coll Cardiol Imaging 2009;2:751-8.
13. Fiechter M, Ghadri JR, Gebhard C, et al. Diagnostic value of ^{13}N-ammonia myocardial perfusion PET: Added value of myocardial flow reserve. J Nucl Med 2012;53:1230-4.
14. Kajander S, Joutsiniemi E, Saraste M, et al. Clinical value of absolute quantification of myocardial perfusion with ^{15}O-water in coronary artery disease. Circ Cardiovasc Imaging 2011;4:678-84.
15. Danad I, Uusitalo V, Kero T, et al. Quantitative assessment of myocardial perfusion in the detection of significant coronary artery disease: Cutoff values and diagnostic accuracy of quantitative [^{15}O]H_2O PET imaging. J Am Coll Cardiol 2014;64:1464-75.
16. Ziadi MC, deKemp RA, Williams K, et al. Does quantification of myocardial flow reserve using rubidium-82 positron emission

tomography facilitate detection of multivessel coronary artery disease? J Nucl Cardiol 2012;19:670-80.
17. Naya M, Murthy VL, Taqueti VR, et al. Preserved coronary flow reserve effectively excludes high-risk coronary artery disease on angiography. J Nucl Med 2014;55:248-55.
18. Gibbons RJ, Balady GJ, Beasley JW, et al. ACC/AHA guidelines for exercise testing. A report of the American College of Cardiology/American Heart Association Task Force on Practice Guidelines (Committee on Exercise Testing). J Am Coll Cardiol 1997;30:260-311.
19. Gould KL, Pan T, Loghin C, Johnson NP, Guha A, Sdringola S. Frequent diagnostic errors in cardiac PET/CT due to misregistration of CT attenuation and emission PET images: A definitive analysis of causes, consequences, and corrections. J Nucl Med 2007;48:1112-21.
20. Ficaro EP, Lee BC, Kritzman JN, Corbett JR. Corridor4DM: The Michigan method for quantitative nuclear cardiology. J Nucl Cardiol 2007;14:455-65.
21. Lee BC, Moody JB, Poitrasson-Rivière A, et al. Blood pool and tissue phase patient motion effects on ^{82}rubidium PET myocardial blood flow quantification. J Nucl Cardiol 2018;26:1918-29.
22. Slomka PJ, Nishina H, Berman DS, et al. Automated quantification of myocardial perfusion SPECT using simplified normal limits. J Nucl Cardiol 2005;12:66-77.
23. Hove JD, Iida H, Kofoed KF, Freiberg J, Holm S, Kelbaek H. Left atrial versus left ventricular input function for quantification of the myocardial blood flow with nitrogen-13 ammonia and positron emission tomography. Eur J Nucl Med Mol Imaging 2004;31:71-6.
24. Lortie M, Beanlands RSB, Yoshinaga K, Klein R, Dasilva JN, DeKemp RA. Quantification of myocardial blood flow with ^{82}Rb dynamic PET imaging. Eur J Nucl Med Mol Imaging 2007;34:1765-74.
25. Huisman MC, Higuchi T, Reder S, et al. Initial characterization of an ^{18}F-labeled myocardial perfusion tracer. J Nucl Med 2008;49:630-6.
26. Robin X, Turck N, Hainard A, et al. pROC: An open-source package for R and S + to analyze and compare ROC curves. BMC Bioinformatics. 2011;12:77.
27. Youden WJ. Index for rating diagnostic tests. Cancer 1950;3:32-5.
28. McNemar Q. Note on the sampling error of the difference between correlated proportions or percentages. Psychometrika 1947;12:153-7.
29. Leisenring W, Alonzo T, Pepe MS. Comparisons of predictive values of binary medical diagnostic tests for paired designs. Biometrics 2000;56:345-51.
30. Fox J, Weisberg S. An R companion to applied regression. 3rd ed. Thousand Oaks: SAGE Publications, Inc; 2018.
31. Harrell FE Jr. Regression modeling strategies. 2nd ed. Cham: Springer; 2015.
32. Fox J, Weisberg S. Visualizing fit and lack of fit in complex regression models with predictor effect plots and partial residuals. J Stat Softw 2018;87:1-27.
33. Pencina MJ, D'Agostino RB, Steyerberg EW. Extensions of net reclassification improvement calculations to measure usefulness of new biomarkers. Stat Med 2011;30:11-21.
34. Benjamini Y, Krieger AM, Yekutieli D. Adaptive linear step-up procedures that control the false discovery rate. Biometrika 2006;93:491-507.
35. R Core Team (2012) *R:* A Language and Environment for Statistical Computing. Vienna, Austria: R Foundation for Statistical Computing. http://www.R-project.org/.
36. Millman KJ, Aivazis M. Python for scientists and engineers. Comput Sci Eng 2011;13:9-12.
37. Gould KL, Johnson NP, Bateman TM, et al. Anatomic versus physiologic assessment of coronary artery disease. Role of coronary flow reserve, fractional flow reserve, and positron emission tomography imaging in revascularization decision-making. J Am Coll Cardiol 2013;62:1639-53.
38. Uren NG, Melin JA, De Bruyne B, Wijns W, Baudhuin T, Camici PG. Relation between myocardial blood flow and the severity of coronary-artery stenosis. N Engl J Med 1994;330:1782-8.
39. Di Carli M, Czernin J, Hoh CK, et al. Relation among stenosis severity, myocardial blood flow, and flow reserve in patients with coronary artery disease. Circulation 1995;91:1944-51.
40. Yoshinaga K, Katoh C, Manabe O, et al. Incremental diagnostic value of regional myocardial blood flow quantification over relative perfusion imaging with generator-produced rubidium-82 PET. Circ J 2011;75:2628-34.
41. Murthy VL, Bateman TM, Beanlands RS, et al. Clinical quantification of myocardial blood flow using PET: Joint position paper of the SNMMI Cardiovascular Council and the ASNC. J Nucl Cardiol 2017;59:273-93.
42. Murthy VL, Naya M, Foster CR, et al. Improved cardiac risk assessment with noninvasive measures of coronary flow reserve. Circulation 2011;124:2215-24.
43. Gupta A, Taqueti VR, van de Hoef TP, et al. Integrated noninvasive physiological assessment of coronary circulatory function and impact on cardiovascular mortality in patients with stable coronary artery disease. Circulation 2017;136:2325-36.
44. Bom MJ, van Diemen PA, Driessen RS, et al. Prognostic value of [^{15}O]H_2O positron emission tomography-derived global and regional myocardial perfusion. Eur Heart J 2019. https://doi.org/10.1093/ehjci/jez258.
45. Murthy VL, Naya M, Taqueti VR, et al. Effects of sex on coronary microvascular dysfunction and cardiac outcomes. Circulation 2014;129:2518-27.
46. Taqueti VR, Shaw LJ, Cook NR, et al. Excess cardiovascular risk in women relative to men referred for coronary angiography is associated with severely impaired coronary flow reserve, not obstructive disease. Circulation 2017;135:566-77.
47. Chareonthaitawee P, Kaufmann PA, Rimoldi O, Camici PG. Heterogeneity of resting and hyperemic myocardial blood flow in healthy humans. Cardiovasc Res 2001;50:151-61.
48. Duvernoy CS, Meyer C, Seifert-Klauss V, et al. Gender differences in myocardial blood flow dynamics: Lipid profile and hemodynamic effects. J Am Coll Cardiol 1999;33:463-70.
49. Danad I, Raijmakers P, Appelman Y, et al. Coronary risk factors and myocardial blood flow in patients evaluated for coronary artery disease: A quantitative [^{15}O]H_2O PET/CT study. Eur J Nucl Med Mol Imaging 2012;39:102-12.
50. Schelbert HR. Positron emission tomography of the heart: Methodology, findings in the normal and the diseased heart, and clinical applications. In: Phelps ME, editor. PET: Molecular imaging and its biological applications. 1st ed. New York: Springer; 2004. p. 389–508.
51. Knaapen P. Quantitative myocardial blood flow imaging: Not all flow is equal. Eur J Nucl Med Mol Imaging 2014;41:116-8.
52. Danad I, Raijmakers PG, Appelman YE, et al. Hybrid imaging using quantitative $H_2^{15}O$ PET and CT-based coronary angiography for the detection of coronary artery disease. J Nucl Med 2013;54:55-63.
53. Nesterov S, Han C, Mäki M, et al. Myocardial perfusion quantitation with ^{15}O-labelled water PET: High reproducibility of the new cardiac analysis software (Carimas^{TM}). Eur J Nucl Med Mol Imaging 2009;36:1594-602.